Supporting Information

HTL-Free $Sb_2(S, Se)_3$ Solar Cells with an Optimal Detailed Balance Band Gap

Yue Lu[†,‡,§], Kanghua Li[†,§], Xuke Yang[†], Shuaicheng Lu[†], Sen Li[†], Jiajia Zheng[†,‡], Liuchong Fu[†], Chao Chen[*,†], Jiang Tang[**,†]

[†]Wuhan National Laboratory for Optoelectronics and School of Optical and Electronic Information, Huazhong University of Science and Technology, Wuhan 430074, Hubei, China

[‡] China-EU Institute for Clean and Renewable Energy, Huazhong University of Science and Technology, Wuhan 430074, Hubei, China

[*]email:Email: cchen@mail.hust.edu.cn.

[**]email:Email: jtang@mail.hust.edu.cn.

Saturated vapor pressure curves of Sb_2Se_3 and Sb_2S_3 sources.

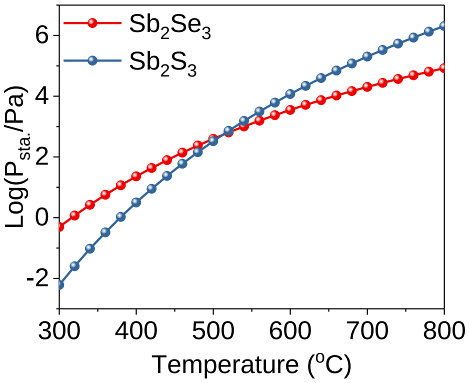

Figure S1. Temperature-dependent saturated vapor pressure of Sb_2Se_3 and Sb_2S_3 in the temperature range from 300 °C to 800 °C.

The temperature-time curves of Sb_2Se_3 and Sb_2S_3 sources.

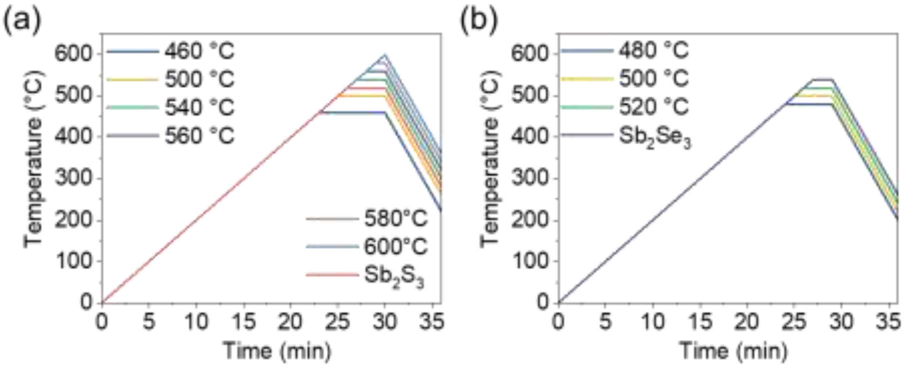

Figure S2. The temperature-time curves of Sb_2Se_3 and Sb_2S_3 sources when adjusted the evaporation temperatures of (a) Sb_2Se_3 and (b) Sb_2S_3.

Top-view SEM images at different Sb_2Se_3 source temperatures.

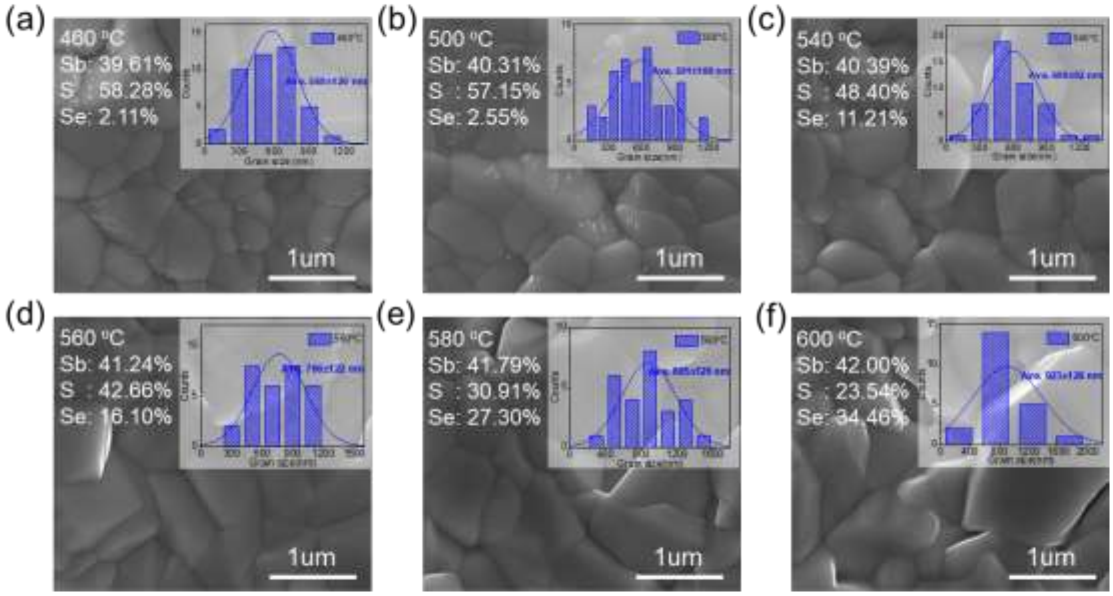

Figure S3. The top-view SEM images of the $Sb_2(S, Se)_3$ films under Sb_2Se_3 source temperature of (a) 460 ºC, (b) 500 ºC, (c)540 ºC, (d) 560 ºC, (e) 580 ºC, (f) 600 ºC. The average grain size are 569±120 nm, 591±100 nm, 609±92 nm, 766±122 nm, 885±126 nm, and 923±128 nm, respectively.

XRD diffraction pattern under different Sb_2Se_3 source temperatures.

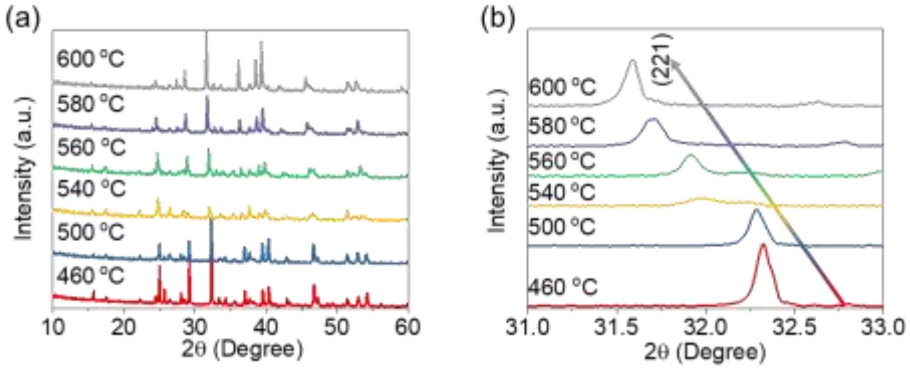

Figure S4. (a) The XRD of the $Sb_2(S, Se)_3$ films and (b) the enlarged [221] peaks of the $Sb_2(S, Se)_3$ films under different evaporating temperatures of the Sb_2Se_3 source.

Transmission spectroscopy at different Sb_2Se_3 source temperatures.

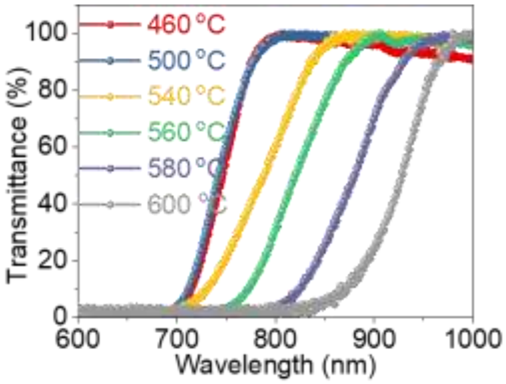

Figure S5. The UV-vis-NIR transmission spectroscopy of $Sb_2(S, Se)_3$ films under different evaporating temperatures of the Sb_2Se_3 source.

Top-view SEM images at different Sb_2S_3 source temperatures.

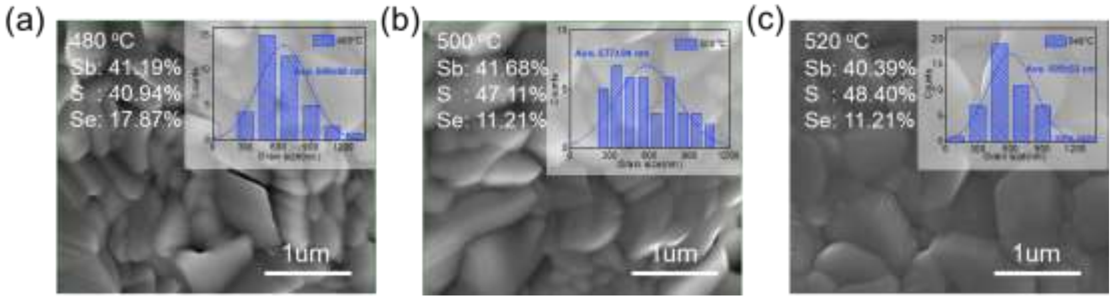

Figure S6. The top-view SEM images of $Sb_2(S, Se)_3$ films under Sb_2S_3 source temperature of (a) 480 ºC, (b) 500 ºC, (c) 520 ºC. The average grain size are 649±90 nm, 577±94 nm, and 609±92 nm, respectively.

XRD diffraction pattern at different Sb_2S_3 source temperatures.

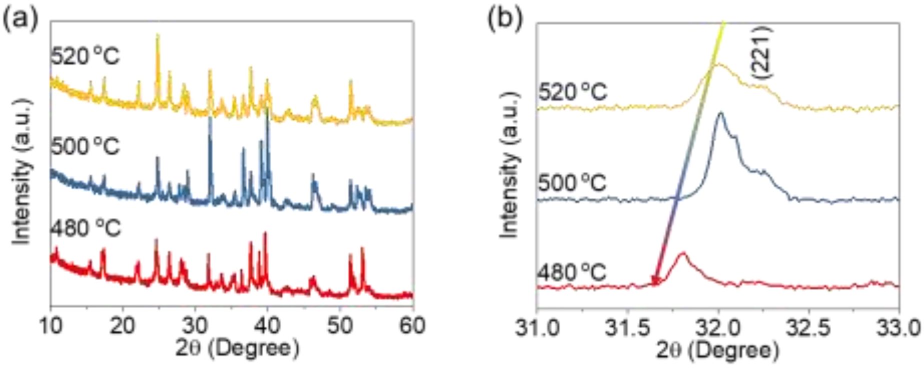

Figure S7. (a) The XRD of the $Sb_2(S, Se)_3$ films and (b) the enlarged [221] peaks of the $Sb_2(S, Se)_3$ films under different evaporating temperatures of the Sb_2S_3 source.

Transmission spectroscopy under different Sb_2S_3 source temperatures.

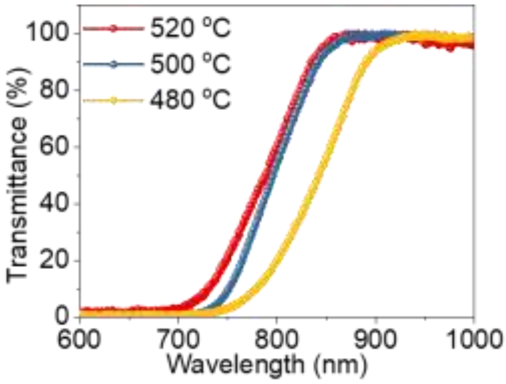

Figure S8. The UV-vis-NIR transmission spectroscopy of $Sb_2(S, Se)_3$ films under different evaporating temperatures of the Sb_2S_3 source.

Schematic diagram of thin film light absorption.

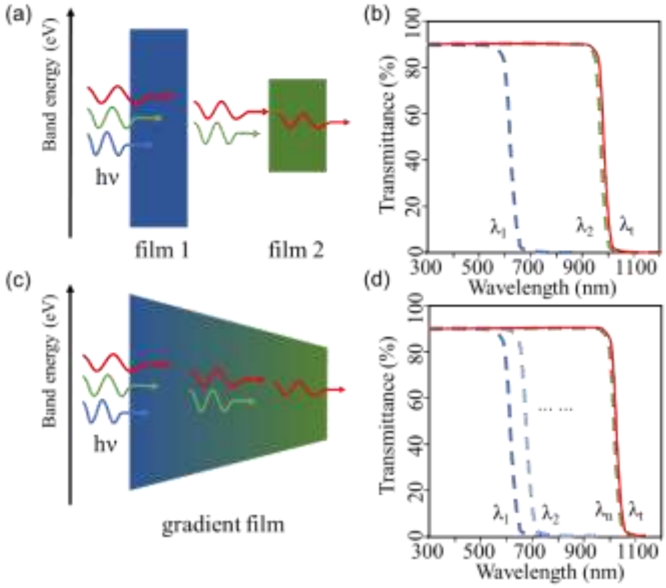

Figure S9. Schematic diagram of a beam of light passing through (a) two layers of films and (c) a gradient film. The schematic transmittance curves of (b) two layers of films and (d) a gradient film.

As shown in Figure S9a, when a beam of light separately passes through two films with different bandgaps, only high-energy photons are absorbed by the wide-bandgap film, and the absorption cutoff edge is expressed as λ_1. Whereas, the low-energy photons can further be absorbed by the thin film with a narrow bandgap, and the absorption cutoff edge is expressed as λ_2. When the light continuously passes through two layers of films, the absorption cutoff edge (expressed as λ_t) is the same as that of the narrow bandgap film (Figure S9b). Further, when a beam of light continuously passes through a multilayer film (gradient bandgap film is the limiting case) (Figure S9c), high-energy photons are absorbed by the wide bandgap materials (λ_1, λ_2…), and only photons with energy lower than the narrowest bandgap are transmitted. Hence, the absorption cutoff edge (expressed as λ_t) is similar to that of the narrowest bandgap film (expressed as λ_n) (Figure S9d). As a result, the fitted bandgap through Tauc plot is determined by the narrowest bandgap in the film.

The heating process of the uniform $Sb_2(S, Se)_3$ films and bandgaps of $Sb_2(S, Se)_3$ films.

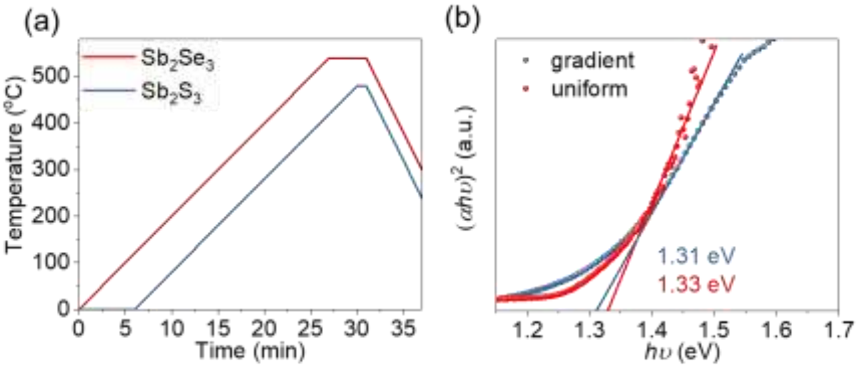

Figure S10. (a) The heating process of the uniform $Sb_2(S, Se)_3$ films. (b) Tauc plot of the gradient and uniform $Sb_2(S, Se)_3$ films.

$1/C^2$-V curves of the devices.

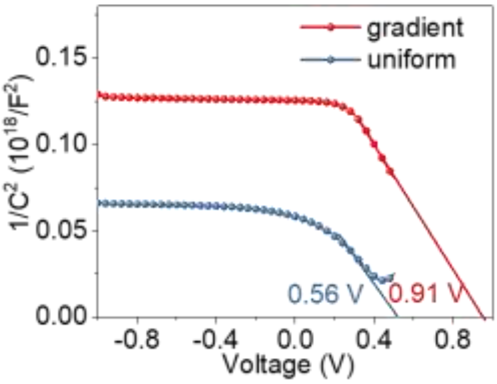

Figure S11. $1/C^2$-V curves of the devices based on gradient and uniform $Sb_2(S, Se)_3$ films. The V_{bi} is 0.56 V and 0.91 V, respectively.

The bandgaps of the devices obtained from EQE data.

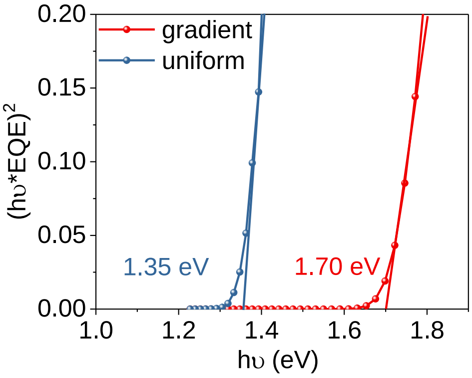

Figure S12. The bandgap of the devices based on gradient and uniform $Sb_2(S, Se)_3$ film obtained from EQE data.

The *J*-*V* curves under different light intensities.

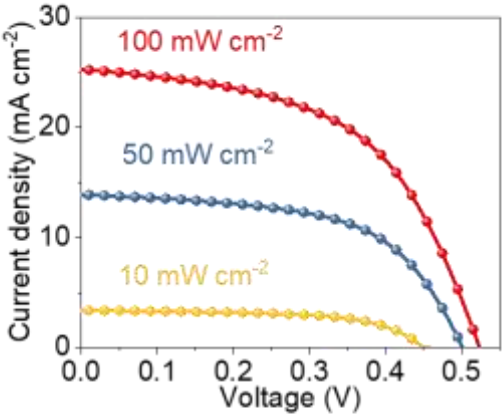

Figure S13. The *J*-*V* curves of the optimal device under different light intensities.

Atomic and ionic radius.

Table S1. The Atomic and Ionic Radius of Sulfur and Selenium.[1]

Radius	S (pm)	Se (pm)
Atomic radius (M)	104	117
Ionic radius (M^{2-})	184	198

Material parameters for SCAPS simulation.

Table S2. The Basic Material Parameters for SCAPS Simulation in $Sb_2(S, Se)_3$ Solar Cells[2-3]

Parameter	SnO_2	CdS	$Sb_2(S, Se)_3$
Relative dielectric constant (ε_r)	9	10	15
Bandgap (eV)	3.6	2.4	1.3
Electron Affinity (eV)	4.0	4.0	4.15
Electron mobility ($cm^2\ V^{-1}\ s^{-1}$)	100	100	10
Hole mobility ($cm^2\ V^{-1}\ s^{-1}$)	25	25	1
N_c (cm^{-3})	2.2×10^{18}	2.2×10^{18}	1.0×10^{18}
N_v (cm^{-3})	1.8×10^{19}	1.8×10^{19}	1.8×10^{20}
Doping density (cm^{-3})	1.0×10^{18}	1.1×10^{18}	1.0×10^{14}
Thickness (nm)	400	60	800

CdS trap states parameters for SCAPS simulation.

Table S3. The CdS Trap States Parameters for SCAPS Simulation in $Sb_2(S, Se)_3$ Solar Cells[2-3]

Parameter	Defect 1
Defect type	Single acceptor (-/0)
E_t (eV) above E_v	1.2
Electron capture cross section (cm^2)	1.0×10^{-17}
Hole capture cross section (cm^2)	1.0×10^{-12}
N_t (cm^{-3})	1.0×10^{18}

$Sb_2(S, Se)_3$ trap states parameters.

Table S4. The $Sb_2(S, Se)_3$ Trap States Parameters for SCAPS Simulation in $Sb_2(S, Se)_3$ Solar Cells[2-4]

Parameter	**Defect 1**	**Defect 2**	**Defect 3**
Defect type	Single acceptor (-/0)	Single acceptor (-/0)	Single donor (0/+)
E_t (eV) above E_v (below E_c)	0.48	0.71	0.61
Electron capture cross section (cm^2)	1.0×10^{-15}	1.0×10^{-15}	4.0×10^{-13}
Hole capture cross section (cm^2)	1.5×10^{-17}	4.9×10^{-13}	1.0×10^{-15}
N_t (cm^{-3})	1.2×10^{15}	1.1×10^{14}	2.6×10^{14}

References

(1) Speight, J. *Lange's Handbook of Chemistry, Sixteenth Edition*; McGraw-Hill Education, New York, 2005; Vol. 4, pp 654-658.

(2) Li, K.; Lu, Y.; Ke, X.; Li, S.; Lu, S.; Wang, C.; Wang, S.; Chen, C.; Tang, J. Over 7% Efficiency of $Sb_2(S,Se)_3$ Solar Cells via V-Shaped Bandgap Engineering. *Sol. RRL* **2020,** *4*, 2000220.

(3) Chen, C.; Wang, L.; Gao, L.; Nam, D.; Li, D.; Li, K.; Zhao, Y.; Ge, C.; Cheong, H.; Liu, H.; et al. 6.5% Certified Efficiency Sb_2Se_3 Solar Cells Using PbS Colloidal Quantum Dot Film as Hole-Transporting Layer. *ACS Energy Lett.* **2017,** *2*, 2125-2132.

(4) Wen, X.; Chen, C.; Lu, S.; Li, K.; Kondrotas, R.; Zhao, Y.; Chen, W.; Gao, L.; Wang, C.; Zhang, J.; et al. Vapor Transport Deposition of Antimony Selenide Thin Film Solar Cells with 7.6% Efficiency. *Nat. Commun.* **2018,** *9*, 2179.